

P-Delta Mass Rig System for Shake Table Tests of Slender Cantilever Columns

Arash Sangtarashha, & Pedro F. Silva

The George Washington University, Washington, DC, U.S.A.

Rigoberto Burgueño

Michigan State University, East Lansing, U.S.A



15 WCEE
LISBOA 2012

SUMMARY:

This paper presents the design of a mass rig system for shake table testing of slender columns. In the presence of P-delta effects slender columns experience destabilizing moments that can lead to the instability of the test specimen, thus requiring additional safety remediation during testing. In order to address safety and economic concerns, the inertial mass will be placed on a convex surface outside of the shake table and the transfer of the inertial forces will be realized by connecting the top of the columns to the inertial mass by a rigid link. Design of the convex surface was achieved by ensuring that the equations of motion for the inertia mass on the convex surface lead to the same solution as if the mass was placed directly on the column. This paper presents the principles used in deriving the expression for the convex surface alongside with analytical validations.

Keywords: P-delta effects, Mass rig system, Shake table tests, Lagrangian mechanics

1. INTRODUCTION

The research described in this paper is part of a project that focuses on shake table testing of slender reinforced concrete bridge (RC) columns. The tests will provide one of a kind link for investigating the effects that loading protocol and P-delta have on the plastic hinge region and the damage levels of slender RC columns. Because the seismic performance of slender RC columns is largely affected by P-delta effects, special considerations were undertaken in setting up a mass rig system. A literature review shows that three different mass rig set ups have been used for shake table tests. In approach the mass is directly connected and placed to the top of the column. One of the main disadvantages of this setup is that the mass needs to be removed and reinstalled between tests leading to delays. Additionally, considerations must be ensured for safety during and after testing in the occurrence of large displacements, or a likely collapse of the specimen. Other systems have averted this disadvantage by placing the mass on a tower that is either placed next to the test specimen on the shake table or on a tower located outside of the shake table. However, because the mass is placed on a flat surface these systems have the main disadvantage of not being able to reproduce or properly quantify P-delta effects on the test specimens.

The need to evaluate P-delta effects on the seismic response of slender RC columns led the research team to design an alternative test setup that places the mass on a steel tower outside of the shake table but the mass moves on a convex surface. The surface profile is designed to properly simulate the directional effects of the gravity loads. In addition, the axial load effects on the internal response of the RC columns will be achieved by internally post-tensioning the test specimens. This construction detail will insure the effects of axial load on the flexural capacity of the section. The curved path was designed by ensuring that the equations of motion for the inertia mass on the convex surface led to the same solution as if the inertia mass was placed on top of the columns. Interfacing the principles of conservation of momentum with conservation of energy in Lagrangian mechanics with state-space

phase analysis led to a simplified derivation of the equations of motion and its subsequent implementation in the design of the surface profile. The paper presents a brief description of the principles used in deriving the expressions for the design of the convex surface alongside with analytical validations.

2. MOTIVATION FOR THE RESEARCH

Much research has been conducted to date on calibrating/validating the plastic-hinge length in reinforced concrete (RC) columns. Three of the most recent models for plastic-hinge length are those proposed by Hines et al. (2004), Berry et al. (2008), and Bae and Bayrak (2008). Among other variables, these models have certainly recognized the importance of spread of plasticity in computing the plastic-hinge length; however, some salient questions remain. One is: is it over conservative or under- conservative to predict the correct length of the plastic hinge? One other is: how much does this error actually matter in evaluating the response of bridges? Finally: for which applications does the error become significant either in terms of design or assessment? Certainly the last question deals with conditions for which P-delta effects can play a significant role in the study of the instability of slender RC columns.

Evaluation of RC bridge columns using one of these models shows that reducing the plastic-hinge length leads to underestimating damage, and that the level of error prediction in assessing damage is greater for RC slender columns. Meanwhile, careful evaluation of commonly used plastic-hinge models shows a wide scatter against experimental data and it can be shown that assessment parameters computed using these models do not comply reasonably well with the intended damage level. This is more evident when applied to limit states other than ultimate – the state at which most models were calibrated. These issues are concerning because slender RC bridge columns are often part of complex and critical components of transportation interstate systems in dense urban areas, and any unintended damage to these columns can lead to severe damage and disruption. As such, it is necessary to properly include the P-delta effects on the shake table testing of slender RC bridge columns.

2.1. Shake table tests of RC bridge columns

As previously discussed, many shake table tests on cantilever RC columns have been conducted by placing the inertial mass on top of the column and subjecting it to the intended ground motion. Among these are the shake table experiments performed on cantilever RC columns by MacRae et al (1994), Mahin et al. (2006), Sakai et al. (2006) [shown in Figure 1(a)], Mosalam et al. (2002), and a recent full-scale test Guerrini et al. (2011) [shown in Figure 1(b)]. Although placing the mass on top of the test specimen has been widely used, its use to the study slender columns can lead to major safety concerns. The concern increases when high inertial and axial loads are being applied to the test specimen or the performance of the column is being investigated to high damage levels. As seen in Figure 1(b) the configuration and size of the inertial mass can be rather large as compared to the test specimen, which can also lead to rotational deformation demands at the top of the column.

As shown in Figure 1(c), Laplace et al. (1999) proposed a different setup in which the inertial mass was placed next to the shake table. This mass rig system is basically a horizontally constraint-free mechanism to provide the inertial dynamic loading during the testing procedure. The axial load applied to the specimen is provided through a steel spreader beam that was attached to the top of the column. The column top displacement is transferred to the mass with a rigid link. Restraining cables are provided to limit the translation of the inertial mass to reduce safety concerns when a test specimen fails. Another advantage of this system is that it also allows specimens to be removed and replaced easily making the installations faster and more convenient.

Although this mass rig system removes several concerns related to shake table testing of cantilever columns, some issues remain that are related to the proper representation of P-delta effects. This indeed was observed during the experiments of Laplace et al. (1999), which showed that the

experimentally derived P-delta force was lower than predicted for the condition when the mass is on top of the column. It is logically anticipated that this inaccuracy will be amplified when the axial load or column aspect ratio increases, causing more significant P-delta effects.



Figure 1: Different inertial loading systems used in shake table experiments on RC cantilever columns

3. DEVELOPMENT AND SOLUTION OF THE EQUATIONS OF MOTION

In the test setup developed for this research the inertial mass is placed on a convex surface outside of the shake table and the transfer of inertial forces is achieved by connecting the top of the column to the inertial mass by a rigid link. A schematic of this setup is shown in Figure 2(a). Based on this setup the motion of mass, m , will take place along a curved path of radius, R , and the the application of Newton's second law in deriving the equations of motion will be a rather complex and cumbersome task since the expressions for all known forces must be properly quantified and expressed in vector notation. As such, *Lagrangian* mechanics was used to simplify the derivation of the equations of motion. This approach is more suitable for this research because it is based on: (1) energy, which is a scalar quantity leading to a series of simpler approaches in deriving the equations of motion, and (2) generalized coordinates rather than the limiting rectangular, polar, or spherical coordinates.

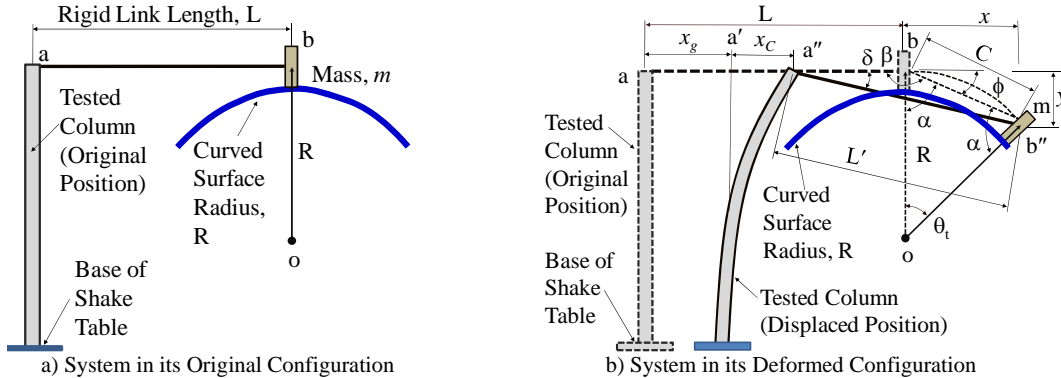


Figure 2. System Schematics in its Original and Deformed Configurations

3.1. Position Equations

The expressions necessary for developing the *Lagrangian* and the rationale for the development of the *Lagrangian* equations are discussed next. The position of the mass m , in its original and deformed configurations can be easily described in terms of polar coordinates and other relevant expressions. Referring to Figure 2(b), segment $\overline{bb''}$ is defined as the chord length, C , of angle θ_t along the curved path and is given by:

$$C = 2R \sin(\theta_t / 2) \quad (3.1)$$

In Eq. (3.1), θ_t is the angle between segments \overline{ob} and $\overline{ob''}$, R is the radius of the curved surface, b defines the original position of mass m , and b'' defines the displaced position of mass m . By the law of cosines the distance of segment $\overline{a''b''}$ is given by:

$$L' = L = (L - x_C - x_g)^2 + C^2 - 2(L - x_C - x_g)C \cos(\beta) \quad (3.2)$$

Where β is the angle between line segments \overline{ab} and $\overline{bb''}$, x_C is the relative horizontal displacement of the column, and x_g is the absolute displacement at the base of the shake table. Solving for $x_C + x_g$ in Eq. (3.2) one obtains:

$$x_C + x_g = L - \sqrt{L^2 - 4R^2 \sin(\theta_t / 2)^2 + R^2 \sin(\theta_t)^2} + R \sin(\theta_t) \quad (3.3)$$

In this last expression the angle β is related to θ_t by $\beta = \pi - \theta_t / 2$. As such, the absolute horizontal and vertical displacements of mass m are, respectively:

$$x = C \cos(\phi) = 2R \sin(\theta_t / 2) \cos(\theta_t / 2) = R \sin(\theta_t) \quad (3.4)$$

$$y = C \sin(\phi) = 2R \sin(\theta_t / 2) \sin(\theta_t / 2) = R [1 - \cos(\theta_t)] \quad (3.5)$$

Where ϕ is the positive angle formed by line segment $\overline{bb''}$ and the horizontal line \overline{ab} . Differentiating these last equations with respect to time one obtains:

$$\dot{x} = R\dot{\theta} \cos(\theta_t) \quad \dot{y} = R\dot{\theta} \sin(\theta_t) \quad \dot{x}_C = \lambda R\dot{\theta} \cos(\theta_t / 2) - \dot{x}_g \quad (3.6)$$

In order to further simplify the complexity of the equations of motion the following equalities were employed:

$$x_C + x_g = \lambda C \Rightarrow x_C = \lambda C - x_g \quad (3.7)$$

$$\lambda = \frac{x_C + x_g}{C} = \frac{L - \sqrt{L^2 - 4R^2 \sin(\theta_t / 2)^2 + R^2 \sin(\theta_t)^2} + R \sin(\theta_t)}{2R \sin(\theta_t / 2)} \quad (3.8)$$

Eq. (3.8) can be solved graphically for λ and it is nearly 1.00 for most of the values of θ , where θ is graphically depicted in Figure 3. Substituting Eq. (3.1) into Eq. (3.5) and solving for x_C leads to:

$$x_C = \lambda 2R \sin(\theta_t / 2) - x_g \quad (3.9)$$

3.2. Energy equations

Assuming the mass of the tested column and rigid link, L , are relatively smaller than mass m , and using the position equations, the kinetic energy, T , of the system is given in terms of Eq. (3.10). Per Eq. (3.11) the potential energy, U , of the system consists of the changes in the potential energy stored in the deformed column and the changes in the gravitational potential of mass m .

$$T = \frac{1}{2} m (\dot{x}^2 + \dot{y}^2) = \frac{1}{2} m R^2 \dot{\theta}^2 [\cos(\theta_t)^2 + \sin(\theta_t)^2] = \frac{1}{2} m R^2 \dot{\theta}^2 \quad (3.10)$$

$$U = \frac{1}{2} K x_C^2 - mgy = \frac{1}{2} K [\lambda 2R \sin(\theta_t / 2) - x_g]^2 - mgR [1 - \cos(\theta_t)] \quad (3.11)$$

Assuming friction losses due to motion of the mass, m , along the curved path, and due to the connections of rigid link to the column and mass are related the velocity at the tip end of column, the energy loss due to the damping energy, D , of the system is computed per Eq. (3.12).

$$D = \frac{1}{2} c \dot{x}_C^2 = \frac{1}{2} c [\lambda R \dot{\theta} \cos(\theta_t / 2) - \dot{x}_g]^2 \quad (3.12)$$

where c is the damping constant, and for this work can be related to a small effective damping ratio of $\xi=2\%$

3.3 Lagrangian equations of motion

Finally the *Lagrangian* is:

$$L = T - U = \frac{1}{2} m R^2 \dot{\theta}^2 - \frac{1}{2} K [\lambda 2R \sin(\theta_t / 2) - x_g]^2 + mgR [1 - \cos(\theta_t)] \quad (3.13)$$

In terms of the *Lagrangian*, the classical equations of motion are given by the *Euler-Lagrange* equation:

$$\frac{d}{dt} \left(\frac{\partial L}{\partial \dot{q}_i} \right) - \frac{\partial L}{\partial q_i} + \frac{\partial D}{\partial \dot{q}_i} = F_i \quad \text{Note: } F_i \text{ is zero.} \quad (3.14)$$

Substitution of Eqs. (3.9), (3.10), (3.11), and (3.12) into *Lagrange's* Eq. (3.14) leads to the sequence of equations that will be used to formulate the equations of motion of mass m along the curved path:

$$\frac{\partial L}{\partial \dot{q}_i} = m R^2 \dot{\theta} \quad \text{and} \quad \frac{d}{dt} \left(\frac{\partial L}{\partial \dot{q}_i} \right) = \frac{d}{dt} (m R^2 \dot{\theta}) = m R^2 \ddot{\theta} \quad (3.15)$$

$$-\frac{\partial L}{\partial q_i} = (K \lambda^2 R - mg) R \sin(\theta_t) - K \lambda R \cos(\theta_t / 2) x_g \quad (3.16)$$

$$\frac{\partial D}{\partial \dot{q}_i} = \frac{1}{2} c \lambda^2 R^2 \dot{\theta} [\cos(\theta_t) + 1] - c \lambda R \cos(\theta_t / 2) \dot{x}_g \quad (3.17)$$

These equations lead to the following 2nd order nonlinear differential equation of motion:

$$m R^2 \ddot{\theta} + \frac{1}{2} c \lambda^2 R^2 [\cos(\theta + \Omega) + 1] \dot{\theta} + (K \lambda^2 R - mg) R \sin(\theta + \Omega) = (c \dot{x}_g + K x_g) \lambda R \cos[(\theta + \Omega) / 2] \quad (3.18)$$

Because θ is the variable of integration, θ_t must be replaced by $\theta_t = \theta + \Omega$, where θ is the variable of integration and Ω is the angle resulting solely from the displacement of the shake table, as is schematically shown in Figure 4. It is important to emphasize that these equations are nonlinear due to the presence of the trigonometric functions. Furthermore, they are coupled because of the coupling of θ and $\dot{\theta}$ in the term $[\cos(\theta + \Omega) + 1] \dot{\theta}$. This poses another challenge in the solution of the problem, and the approach used to solve the equations of motion is outlined next.

3.3. Numerical solution and response of the system

The equations of motion depicted in Eq. (3.18) were solved by introducing the *state vector* shown in Eq. (3.19), in terms of the state variables x_1 and x_2 . Employing this *state space* it is possible to obtain the system of first order nonlinear differential equations expressed in Eq. (3.20). Solutions in terms of the state variables x_1 and x_2 can be obtained by solving the system of first-order nonlinear differential equations numerically using a subroutine in MATLAB®. The MATLAB® ODE113 solver was employed for the numerical solution because problems of the type given by Eq. (3.20) are computationally intensive problems and are best solved using this solver.

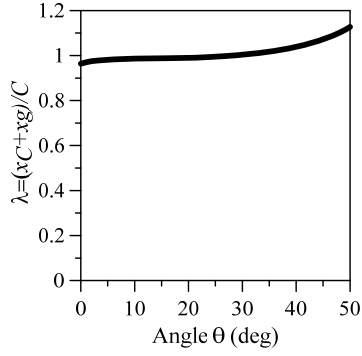


Figure 3. Graphical Representation of λ

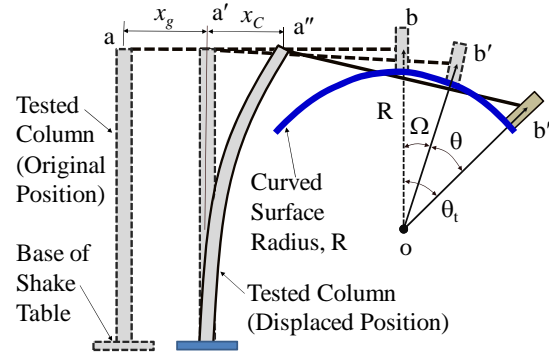


Figure 4. Relations for θ_t as a Function of θ and Ω

Within the solution algorithm the displacement at the tip of the column is computed iteratively using the base displacement, x_g , and base velocity, \dot{x}_g , at each increment. As previously stated, in the first iteration λ was assumed equal to 1.00 and in subsequent iterations λ was estimated based on Eq. (3.8). The solution algorithm has been numerically evaluated using the El Centro, CA (1940) record, for which the acceleration, velocity and displacement time histories are presented in Figure 5.

$$\{x(t)\} = \begin{Bmatrix} x_1(t) \\ x_2(t) \end{Bmatrix} = \begin{Bmatrix} \theta(t) \\ \dot{\theta}(t) \end{Bmatrix} \quad (3.19)$$

$$\{\dot{x}\} = \begin{Bmatrix} \dot{x}_1 = x_2 \\ \dot{x}_2 = -\left(\omega_N^2 \lambda^2 - \frac{g}{R}\right) \sin(x_1 + \Omega) - \xi \omega_N \lambda^2 [\cos(x_1 + \Omega) + 1] x_2 \\ \left(2\xi \omega_N \dot{x}_g + \omega_N^2 x_g\right) \lambda / R \cos\left[\frac{(x_1 + \Omega)}{2}\right] \end{Bmatrix} \quad (3.20)$$

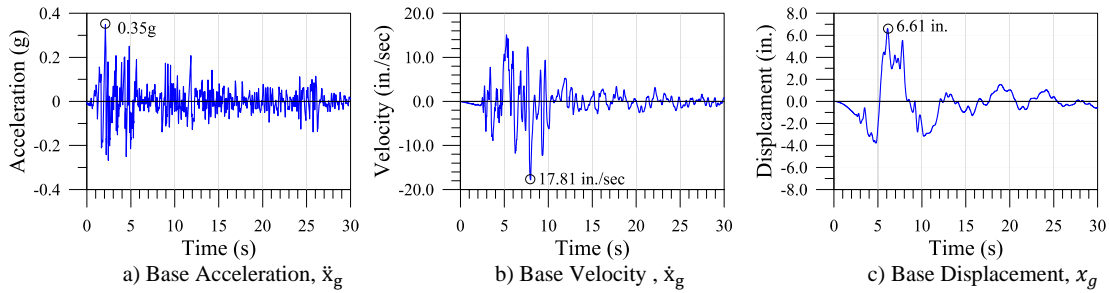


Figure 5: Magnitude 7.1 El Centro Earthquake Record at the USGS station 5054

4. TEST SETUP DESIGN

The surface profile is designed to properly simulate the directional effects of gravity loads. While the proposed test setup is based on the concept of the UNR mass rig system, in this setup, the mass is travelling on a predefined arched path. A schematic diagram for the rig system is presented in Figure 6(a). As shown in Figure 6(b) the inertial mass consists of steel plates that are bolted together and attached to a steel platform that moves along the arched path using a rollercoaster type connection. Different number of steel plates can be easily accommodated to meet the loading requirements and as such changing the period of the system.

As shown, the rollercoaster type connections in each rail consist of three sets of wheels capable of holding the mass from jumping over the arched path. The arched path is created by two tubes that are

manufactured to a smooth finish necessary to minimize the amount of resistance when the wheels move across the tubes. The mass rig system is currently being experimentally evaluated on elastic specimens to within large elastic drift demands. The specimen used to investigate the feasibility of this system will be a thin plate made of ASTM Steel 304, which provides high yield stress and can be used for a large range of elastic displacements. Further details for the construction of mass rig system are provided in Figure 6. The experimental results and comparisons with the analytical solution (presented in this paper) will be available by the time of the conference and presented at that time.

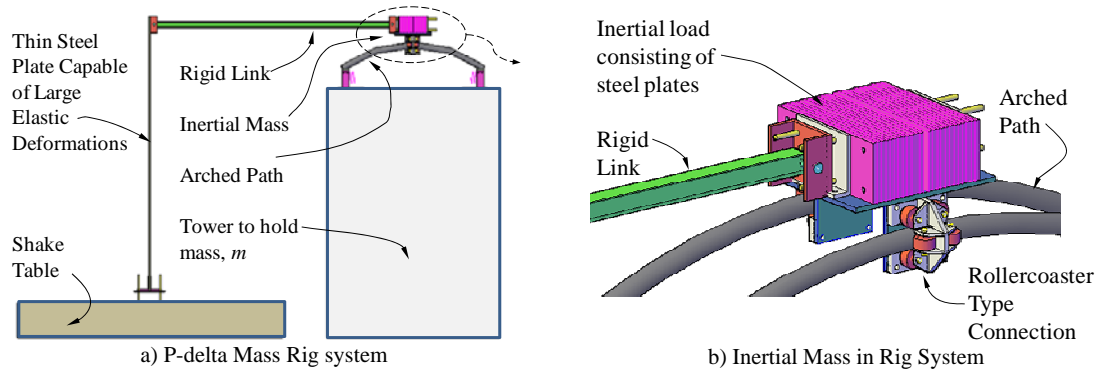


Figure 6: Specifications of the P-delta Mass Rig System

4.1. Response spectrum analysis

In order to select a single radius that suits the majority of testing cases, a series of analysis were performed with different radii and based on the results, a radius of 170 in. was found to be the best fit for the selected range of applications. The single radius selection was achieved by comparing the difference in the analytical results “with” and “no” P-delta transformations on the stiffness matrix. Solution to the equation of motion given by Eq. (3.20) was repeated for radii in 10in. increments, considering the fact that for dimensions of this test setup, an increase of 10in. in radius for the curve results in an increase of 0.04in. for the elevation at the midpoint of the rails. The 1940 El Centro earthquake time history record (shown in Figure 5) was selected for the analyses presented in this section. This earthquake is well suited for this research because, as it can be seen from Figure 7, its displacement response spectrum shows a wide range of scenarios that must be accounted for when selecting the best fit radius.

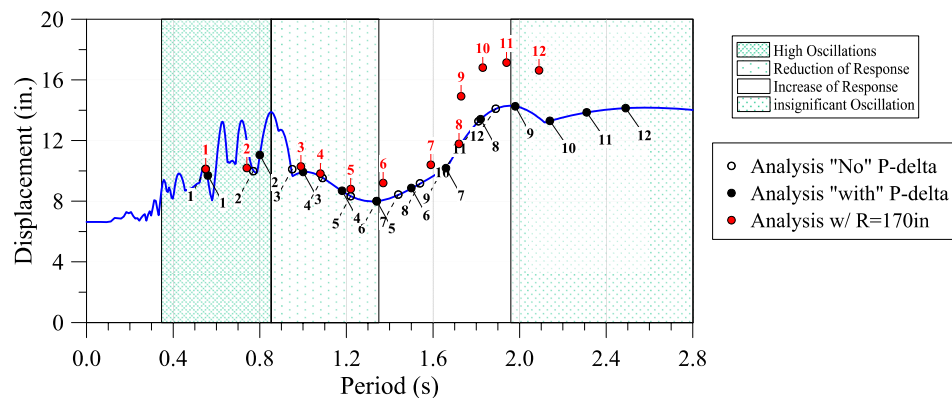


Figure 7: Spectral Displacement of El Centro Earthquake Record

Referring again to Figure 7, it is essential to avoid constructing tests with a natural period less than 0.9 seconds as a small error in predicting the natural period may actually lead to a large fluctuation in the peak response of the structure during testing. For the majority of testing cases and within the range of

natural periods from 1.35s to 2.0s the displacement response spectrum of the El Centro record presents some conditions that make it suitable in selecting the best fit radius for this research. Within this context, the case numbers depicted in Figure 7 are discussed next.

A set of twelve load cases were selected for the analyses with the main objective of varying the natural period of the structure and selecting the best curve fit for the construction of the curved path. These load cases were selected based on varying the number of steel plates for the inertial load as depicted in Figure 6(b). Table 1 presents in the second column the load values in pounds for each of the load cases (i.e., cases 1 to 12) and the corresponding peak results from: (1) the analysis considering No P-delta effects, (2) solving Eq. (3.20) for a large radius of 4800 in., (3) the analysis considering P-delta effects, and (4) solving Eq. (3.20) for a radius of 170 in.

Table 1: Spectral Displacements for Analyses w/ and w/o P-delta Effects

Load Case	Load (lbs)	No P-delta (in)	Radius=4800in (in)	With P-delta (in)	Radius=170in (in)
1	25.52	10.13	10.06	9.70	10.12
2	51.04	9.98	10.03	11.05	10.19
3	76.56	10.11	10.01	9.93	10.29
4	102.08	9.53	9.54	8.69	9.82
5	127.6	8.33	8.34	8.01	8.80
6	153.12	8.00	8.04	8.87	9.20
7	178.64	8.44	8.50	10.18	10.40
8	204.16	9.18	9.26	13.41	11.78
9	229.68	9.97	10.06	14.26	14.92
10	255.2	11.70	11.82	13.30	16.81
11	280.72	13.27	13.43	13.86	17.14
12	306.24	14.10	14.21	14.14	16.63

It is clear that the results in columns 3 and 4 of Table 1 are nearly the same. This is expected as the analyses for a large radius will approximate those cases with a path that is flat, thus providing no directional effects for the inertial mass. Results for the analyses considering No P-delta effects, considering P-delta effects, and for a radius of 170 in. are shown in Figure 7. From this figure it can be seen that those results using a radius of 170 in. can replicate reasonably well the results considering the P-delta effects within case numbers 3 to 8. On the other hand, there is a significant divergence in the results for the remaining of the load cases. This does not necessarily lead to the conclusion that a curve radius of 170 in. cannot duplicate the P-delta effects for these cases, but that for these cases the mass will need to be adjusted accordingly as to match the desired response.

4.2. Selection of the best fit radius for construction of the arched path

Using the results from all the load cases presented in Table 1 a best fit was used to obtain the single radius selection for the construction of the arched path. In this section the spectral displacements obtained for those cases not considering P-delta effects are designated as SD_o and those cases considering P-delta effects are designated as SD_p . Based on this definition the standard deviation between the spectral displacements SD_o and SD_p is designated as σ_{op} and is computed using Eq. (4.1). In this equation σ_{op} is the standard deviation for the difference between SD_{oi} and SD_{pi} . The value of this quantity is shown in Figure 8 as a straight line. Those cases solved in terms of Eq. (3.20) and considering a radius in the range of 60 to 280 in. in increments of 10 in. are designated as SD_R . Likewise, based on this definition the standard deviation between the spectral displacements SD_R and SD_p is designated as σ_{Rp} and is computed using Eq. (4.2).

$$\sigma_{op} = \sqrt{\frac{\sum_{i=1}^n (SD_{oi} - SD_{pi})^2}{n}} \quad (4.1)$$

$$\sigma_{Rp} = \sqrt{\frac{\sum_{i=1}^{12} (SD_{Ri} - SD_{pi})^2}{12}} \quad (4.2)$$

In these equations σ_{Rp} is the standard deviation for the difference between SD_{Ri} and SD_{pi} , and n is the number of cases considered in obtaining the radius that best suits all the load conditions considered for testing. In order to estimate the optimum value for the radius of the arched path, these standard deviations are plotted in Figure 8. Figure 8(a) shows the standard deviation computed using all load cases (1 to 12) in which the number of cases $n=12$. Figure 8(b) shows the standard deviation computed using only load cases 6 to 9, in which the number of cases $n=4$.

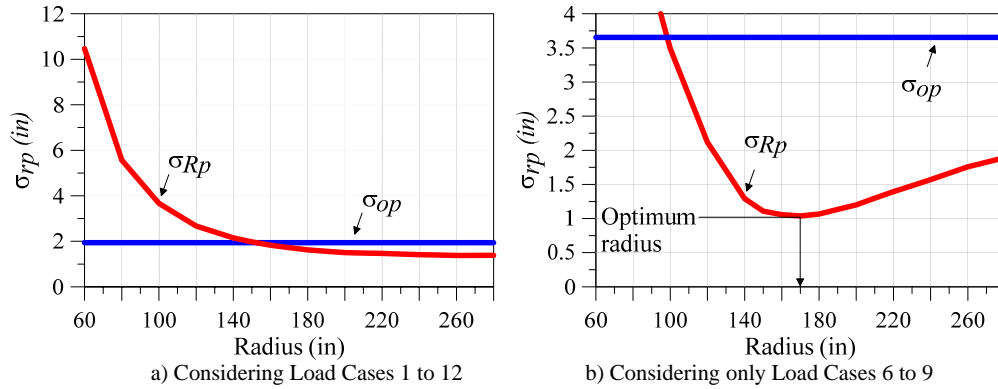


Figure 8: Comparison of Results of Analyses with Different Radiuses Using Standard Deviation

In Figure 8(a) the standard deviation σ_{Rp} does not show an optimum value lower than σ_{op} within the range of the radiuses considered. This indicates that the mass rig system cannot simulate the P-delta effects for the entire range of load cases (i.e., load cases 1 thru 12). This is clearly observed in Figure 7, which shows a pronounced difference in load cases 9 to 12 compared to those results obtained for a radius of 170 in. and the results considering P-delta effects. Since it is not possible to select a radius that fits all load cases it is best to select the radius for those ranges of load cases that are being considered for testing. Certainly, the mass rig system can be constructed such that changing the arched rails is an easy task. Indeed if one needs to consider a curved path that best fits only load cases 6 to 9, the best fit radius for these load cases can be obtained by computing the standard deviation for only these cases. Referring to this figure, the best fit radius was obtained for the minimum value of the standard deviation σ_{Rp} , which for this case was 170 inches.

Using the radius of 170 in. and the loading mass of load case 9 the analyses representative of the following simulations: (1) considering P-delta, (2) not considering P-delta, and (3) solution of Eq. (3.20) using a radius of 170 in. were obtained and results are presented in Figure 9.

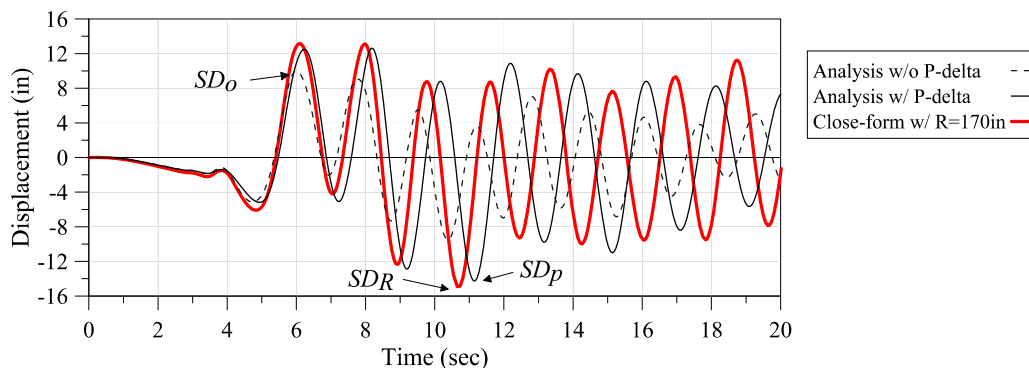


Figure 9: Time-history response for absolute tip column displacement (load case 9)

The natural period of the structure considering P-delta effects was estimated at 1.98 seconds. In this figure the maximum displacements obtained using these three solution methods are designated as SD_p ,

SD_o , and SD_R , respectively. It can be seen that SD_R (solution for a radius of 170 in.) is within a reasonable level of accuracy to SD_p (solution considering P-delta effects). It is also worth noting that both SD_p and SD_R occur on the negative side, while SD_o (solution not considering P-delta effects) is on the positive side of the response. Another salient point is that the solutions considering P-delta effects and the close-form solution for $R=170$ in. diverge after approximately 3 cycles. However, it is important to note that the amplitude of vibration after these first three cycles remains nearly the same for these two analyses.

5. CONCLUSIONS

This paper discussed the analytical approaches and solutions used in designing a mass rig system that can be effectively used in replicating P-delta effects in slender columns. A new mass rig system was proposed and analyzed using the *Lagrangian* equations and *state space* formulation. This inertial loading system may be used in experiments where safety and economic concerns limit the possibility of placing the mass on top of the specimen and P-delta effects are expected to be critical. It is shown that for certain ranges of load applications, in which P-delta has an increasing effect on the maximum displacement of the column, an optimum value for the radius of the arched path can be selected to replicate the P-delta effects very close to the expected results when the mass is placed directly on top of the column.

ACKNOWLEDGEMENT

This project is part of a collaborative research project between the George Washington University and Michigan State University funded by National Science Foundation under grants number and CMS-1000797 and CMS-1000549. The authors gratefully acknowledge the support from Dr. Kishor C. Mehta Director of Hazard Mitigation and Structural Engineering Program at NSF.

REFERENCES

- Bae, S. and Bayrak, O. (2008). Plastic Hinge Length of Reinforced Concrete Columns. *ACI Structural Journal*. **105:3**, 290-300.
- Berry, M.P., Lehman, D.E., and Lowes, L.N. (2008). Lumped-Plasticity Models for Performance Simulation of Bridge Columns. *ACI Structural Journal*. **105:3**, 270-279.
- Hines, E.M., Restrepo, J.I., and Seible, F. (2004). Force-Displacement Characterization of Well-Confined Bridge Piers. *ACI Structural Journal*. **101:4**, 537-548.
- Laplace, P., Sanders, D., Saiidi, M.S. and Douglas, B. (1999). Shake Table Testing of Flexure Dominated reinforced Concrete Bridge Columns. *Center for Earthquake Engineering Research*. **Report No. CCEER-99/13**, University of Nevada, Reno, Nevada, U.S.
- MacRae, G. A., Hodge, C., Priestley, M. J. N. and Seible, F. (1994). Shake Table Tests of As-Built and Retrofitted Configuration. *Structural Systems Research Project*. **Report No. SSRP-94/18**, University of California, San Diego, LaJolla, California, U.S.
- Mahin, S., Sakai, J., and Jeong, H. (2006). Use of partially prestressed reinforced concrete columns to reduce post-earthquake residual displacements of bridges. *Proc., 5th National Seismic Conf. on Bridges and Highways*, MCEER Publications, State University of New York at Buffalo, **Paper No. B25**, 12.
- Mosalam, K.M., Naito, C. and Khaykina, S. (2002). Bidirectional Cyclic Performance of Reinforced Concrete Bridge Column-Superstructure Subassemblies. *Earthquake Spectra*. **18:4**, 663-687.
- Sakai, J., Jeong, H. and Mahin, S. (2006). Reinforced Concrete Bridge Columns that Re-Center Following Earthquakes. *8th National Conference on Earthquake Engineering*. San Francisco, CA, Paper 1421.
- Guerrini, G., Schoettler, M., Restrepo, J.I. (2011). *Large-Scale Validation of Seismic Performance of Bridge Columns*. NEES and MCEER Annual Meeting
http://mceer.buffalo.edu/quakesummit2011/program/presentations/00-Friday%20Plenary_NEES-Showcase_b-Guerrini.pdf